Resource

Cell Reports

A RhoA-FRET Biosensor Mouse for Intravital Imaging in Normal Tissue Homeostasis and Disease Contexts

Graphical Abstract

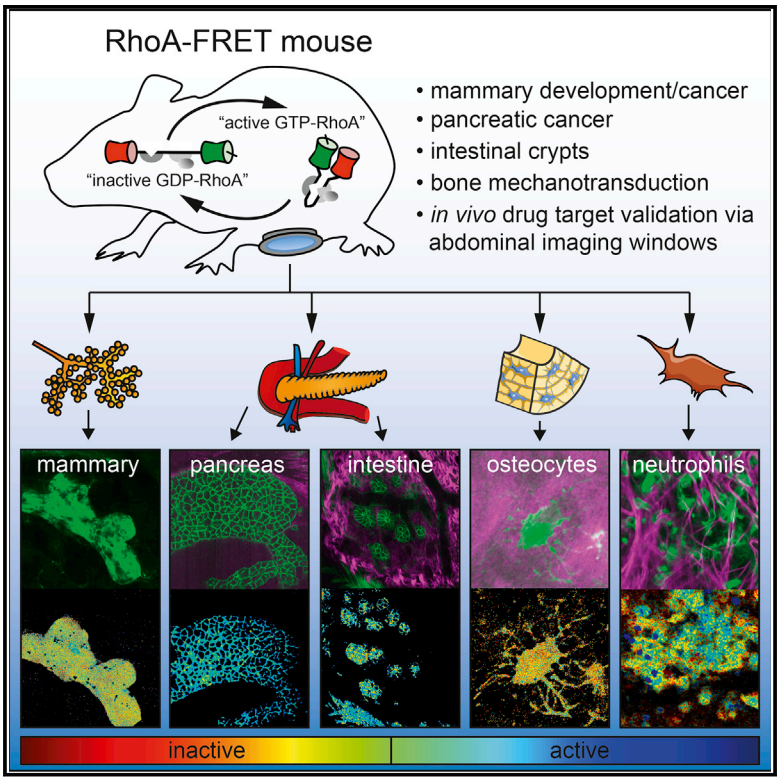

Authors

Max Nobis, David Herrmann, Sean C. Warren, ..., Douglas Strathdee, Kurt I. Anderson, Paul Timpson

Correspondence

kurt.anderson@crick.ac.uk (K.I.A.), p.timpson@garvan.org.au (P.T.)

In Brief

Nobis et al. generated a RhoA-FRET biosensor mouse to characterize and quantify the spatiotemporal distribution of RhoA activity in native mammalian tissues in vivo during development and disease progression. They show that RhoA activity is tightly regulated during various normal biological processes and is co-opted in disease settings, such as invasive breast and pancreatic cancers.

Highlights

- Live quantification of RhoA activity during development and disease progression
- Real-time visualization of RhoA signaling in normal skin, osteocytes, and neutrophils
- Monitoring deregulation of RhoA activity in invasive mammary and pancreatic cancers
- Longitudinal in vivo imaging of RhoA inhibition using optical windows

Nobis et al., 2017, Cell Reports *21*, 274–288
October 3, 2017
https://doi.org/10.1016/j.celrep.2017.09.022

OPEN ACCESS
CellPress

Cell Reports
Resource

A RhoA-FRET Biosensor Mouse for Intravital Imaging in Normal Tissue Homeostasis and Disease Contexts

Max Nobis,[1,10] David Herrmann,[1,10] Sean C. Warren,[1,10] Shereen Kadir,[2] Wilfred Leung,[1] Monica Killen,[1] Astrid Magenau,[1] David Stevenson,[2] Morghan C. Lucas,[1] Nadine Reischmann,[1] Claire Vennin,[1] James R.W. Conway,[1] Alice Boulghourjian,[1] Anaiis Zaratzian,[1] Andrew M. Law,[1] David Gallego-Ortega,[1] Christopher J. Ormandy,[1] Stacey N. Walters,[1] Shane T. Grey,[1] Jacqueline Bailey,[1] Tatyana Chtanova,[1] Julian M.W. Quinn,[1] Paul A. Baldock,[1] Peter I. Croucher,[1] Juliane P. Schwarz,[2] Agata Mrowinska,[2] Lei Zhang,[1] Herbert Herzog,[1] Andrius Masedunskas,[3,4] Edna C. Hardeman,[3] Peter W. Gunning,[4] Gonzalo del Monte-Nieto,[5,6] Richard P. Harvey,[5,6] Michael S. Samuel,[7] Marina Pajic,[1] Ewan J. McGhee,[2] Anna-Karin E. Johnsson,[8] Owen J. Sansom,[2] Heidi C.E. Welch,[8] Jennifer P. Morton,[2] Douglas Strathdee,[2] Kurt I. Anderson,[9,*] and Paul Timpson[1,11,*]

[1]The Garvan Institute of Medical Research, St. Vincent's Clinical School, Faculty of Medicine, University of New South Wales, Sydney, NSW 2010, Australia
[2]Cancer Research UK Beatson Institute, Switchback Road, Bearsden, Glasgow G611BD, UK
[3]Neuromuscular and Regenerative Medicine Unit, University of New South Wales, Sydney, NSW 2010, Australia
[4]Oncology Research Unit, School of Medical Sciences, University of New South Wales, Sydney, NSW 2010, Australia
[5]Developmental and Stem Cell Biology Division, Victor Chang Cardiac Research Institute, Sydney, NSW 2010, Australia
[6]St. Vincent's Clinical School of Biotechnology and Biomolecular Sciences, University of New South Wales, Sydney, NSW 2052, Australia
[7]Centre for Cancer Biology, SA Pathology and University of South Australia School of Medicine, University of Adelaide, Adelaide, SA 5000, Australia
[8]Signalling Programme, Babraham Institute, Cambridge CB223AT, UK
[9]Francis Crick Institute, London NW11AT, UK
[10]These authors contributed equally
[11]Lead Contact
*Correspondence: kurt.anderson@crick.ac.uk (K.I.A.), p.timpson@garvan.org.au (P.T.)
https://doi.org/10.1016/j.celrep.2017.09.022

SUMMARY

The small GTPase RhoA is involved in a variety of fundamental processes in normal tissue. Spatiotemporal control of RhoA is thought to govern mechanosensing, growth, and motility of cells, while its deregulation is associated with disease development. Here, we describe the generation of a RhoA-fluorescence resonance energy transfer (FRET) biosensor mouse and its utility for monitoring real-time activity of RhoA in a variety of native tissues in vivo. We assess changes in RhoA activity during mechanosensing of osteocytes within the bone and during neutrophil migration. We also demonstrate spatiotemporal order of RhoA activity within crypt cells of the small intestine and during different stages of mammary gestation. Subsequently, we reveal co-option of RhoA activity in both invasive breast and pancreatic cancers, and we assess drug targeting in these disease settings, illustrating the potential for utilizing this mouse to study RhoA activity in vivo in real time.

INTRODUCTION

The prototypical Rho GTPases RhoA, Rac1, and Cdc42 play key roles in cellular homeostasis, including in the regulation of cell cycle progression, cell polarity, and cell migration (Hall and Nobes, 2000), which are often hijacked in disease. Rho GTPases are molecular switches that cycle between inactive guanosine diphosphate (GDP)-bound and active guanosine triphosphate (GTP)-bound states. They are activated by guanine nucleotide exchange factors (GEFs), inactivated by GTPase-activating proteins (GAPs), and sequestered to the cytoplasm in their inactivated state by guanine nucleotide dissociation inhibitors (GDIs) (Bishop and Hall, 2000; Cherfils and Zeghouf, 2013; Nobes and Hall, 1999; Zhang et al., 2016).

RhoA is thought to control actomyosin contractility (Wheeler and Ridley, 2004) and regulate cell-cell junction integrity (Braga et al., 1997). RhoA and Rac1 have also been shown to be reciprocally active at the edge of moving cells (Machacek et al., 2009). They act during different modes of migration, with Rac1 activity associated with mesenchymal migration and RhoA with amoeboid migration. Cells can switch between these modes depending on the surrounding tissue topology, demonstrating the plasticity in Rho family GTPase signaling (Byrne et al., 2016; Friedl and Alexander, 2011).

Here we focus on RhoA, which is thought to be a key regulator of normal cellular homeostasis and is often deregulated in a range of disease states. Eloquent work in *Xenopus*, *Drosophila*, and zebrafish has revealed an intricate interplay and compartmentalization of Rho GTPase activity in developmental processes (Kardash et al., 2010; Miyagi et al., 2004; Wang et al., 2010). Deregulation of both upstream and downstream regulators of RhoA in mammalian cells has also been linked to cancer (Rath and Olson, 2012; Rath et al., 2017; Vennin et al., 2017). Moreover, the subcellular and spatiotemporal regulation of RhoA has been associated with invasive pancreatic cancer using

in vivo xenograft models (Timpson et al., 2011), while a differential balance of Rac1 and Cdc42 versus RhoA drives invasion in an orthotopic model of glioblastoma (Hirata et al., 2012). These studies have yielded significant insights into the role and regulation of RhoA in complex 3D disease and model organism settings, illustrating the need for a resource to assess the regulation of RhoA in vivo, both in normal mammalian tissues and in disease models, independently of transfection-based and allograft approaches.

Fluorescence resonance energy transfer (FRET) imaging has emerged as a reliable tool for studying protein-protein interactions (Conway et al., 2017), in particular for transient signaling events that are difficult to access in vivo using conventional methods (Heasman et al., 2010). Here we present the generation of a RhoA-FRET biosensor mouse to study the role of RhoA in tissue homeostasis and disease progression in vivo. We provide spatiotemporal analysis of RhoA activity in a number of tissue-specfic cellular contexts where RhoA is hypothesized to play a role, which have, to date, proved challenging to access by conventional biochemical methods or using transfection-based techniques. We explore the role of RhoA in mechanosensing of osteocytes in situ, and we visualize RhoA activity in neutrophils in vivo in response to local tissue damage. These processes are difficult to recapitulate in an in vitro setting, and they demonstrate the potential of this mouse to probe the role of spatiotemporal regulation of RhoA in cells in their native context. We then combine the RhoA-FRET mouse with optical imaging windows (Ritsma et al., 2012, 2013, 2014) and genetically engineered mouse (GEM) models of cancer to illustrate the fundamental advances the RhoA-FRET mouse can provide in pre-clinical imaging in normal or disease conditions.

RESULTS

Generation and Characterization of the RhoA-FRET Mouse in Normal Tissue

The RhoA-FRET biosensor mouse was generated using a modified EGFP/mRFP Raichu-RhoA biosensor (Timpson et al., 2011; Yoshizaki et al., 2003) (Figure 1A). When RhoA is activated, the RhoA domain of the FRET reporter becomes GTP loaded and binds to the PKN domain, inducing a conformational change that leads to FRET between the two fluorophores (Figure 1A), while GDP loading dissociates the PKN domain binding. The probe is anchored to the membrane by a CAAX box of Ki-Ras, allowing for a subcellular readout of RhoA activity. This probe has been robustly characterized, and its dynamic range has been established in vitro using dominant-negative (T19N) and constitutively active (Q63L) mutants (Timpson et al., 2011). Here, to read out RhoA activity, we used fluorescence lifetime imaging microscopy (FLIM) of the donor fluorophore EGFP, which decreases upon FRET and has been validated in a number of biological contexts (Heasman et al., 2010).

The final targeting vector was generated by inserting a lox-stop-lox transgene under the control of a CAG promoter into the *Hprt* locus. We first generated RhoA-OFF mice, in which expression of the RhoA-FRET biosensor was conditionally prevented by a transcriptional stop sequence (Figures 1B and 1C). We subsequently crossed the RhoA-OFF mice to mice expressing cytomegalovirus (CMV)-Cre recombinase to enable ubiquitous expression of the RhoA-FRET biosensor (termed RhoA-ON mice). Homozygous offspring of both strains were fertile, healthy, showed no abnormal defects, and exhibited the expected Mendelian ratio of hereditary transmission.

In the RhoA-ON mouse, the ubiquitiously expressed biosensor could readily be imaged at depth in normal mammary gland, pancreas, intestine, and neutrophils (Figure 1D; Movie S1, organ z stacks, green; biosensor expression, magenta; second harmonic generation [SHG] of surrounding extracellular matrix [ECM]). Western blot analysis of the RhoA-ON mouse demonstrated low expression levels of the biosensor in a variety of tissues (Figures 1E and 1F; Figures S1A–S1C; Movie S1). RhoA activity was further confirmed using RhoA-GTP immunofluorescence (Figure S2). In the skin, active-RhoA-GTP immunofluorescence is observed in the highly proliferative basal keratinocyte layer of the inter-follicular epidermis and within the hair follicle, aligning with RhoA activity observed in the RhoA-FRET-imaged sections. This is consistent with our previous observation that the RhoA-effector protein ROCK is activated in these regions of the skin (Ibbetson et al., 2013).

A more extensive characterization and expression profile in other organs, or sub-organ-specific settings (Figures S1 and S3; Movie S1), in the RhoA-OFF mouse illustrates the broad capacity for RhoA imaging, ranging from imaging endothelial cells via TEK-Cre and monitoring beta cells within islets of Langerhans using RIP-Cre to imaging neurons via NPY-Cre (Figure S3; Movie S2). The activity of RhoA was also investigated in embryonic skin explants (embryonic day E14.5–E15.5), extracted as described previously (Li et al., 2011), by driving the reporter expression in either keratinocytes using K14-Cre or melanocytes via TyrB-Cre (Figures S4A–S4C; Movie S3). Since Rac1 activation can antagonize the activity of RhoA (Hetmanski et al., 2016; Nimnual et al., 2003), Rac1 and RhoA interplay in melanocyte migration may also be assessed (Figures S4D–S4F). We next characterized RhoA signaling in normal tissue-specific contexts to illustrate the detailed subcellular and spatiotemporal resolution achievable with this RhoA-FRET mouse.

Directional RhoA Activation in Osteocyte Protrusions during Mechanosensing

RhoA signaling has been implicated in the transduction of mechanical signals in osteoblast-like cells (Hamamura et al., 2012). We therefore wanted to investigate the spatiotemporal regulation of RhoA signaling in response to mechanical loading in mature osteocytes, which are embedded in the bone matrix and are thought to transduce force response through the bone (Noble, 2008). Driving RhoA-FRET reporter (RhoA-OFF) expression via the Col1a1.3.6-Cre enabled us to monitor RhoA activity in osteocytes in the calvaria (Figures 2A and 2B; Figures S5A and S5B). Using the RhoA-FRET biosensor mouse, we visualized osteocytes residing within the lacunae of freshly excised calvaria with protrusions spreading through canaliculi of the bone (Figures 2A and 2B; Movie S4, panel 1).

To monitor the role of RhoA signaling in the mechanosensing processes of osteocytes, we applied a compressive force to sections of calvaria along a defined axis during imaging (Figure 2C; Figures S5C–S5E, with schematic). We monitored the

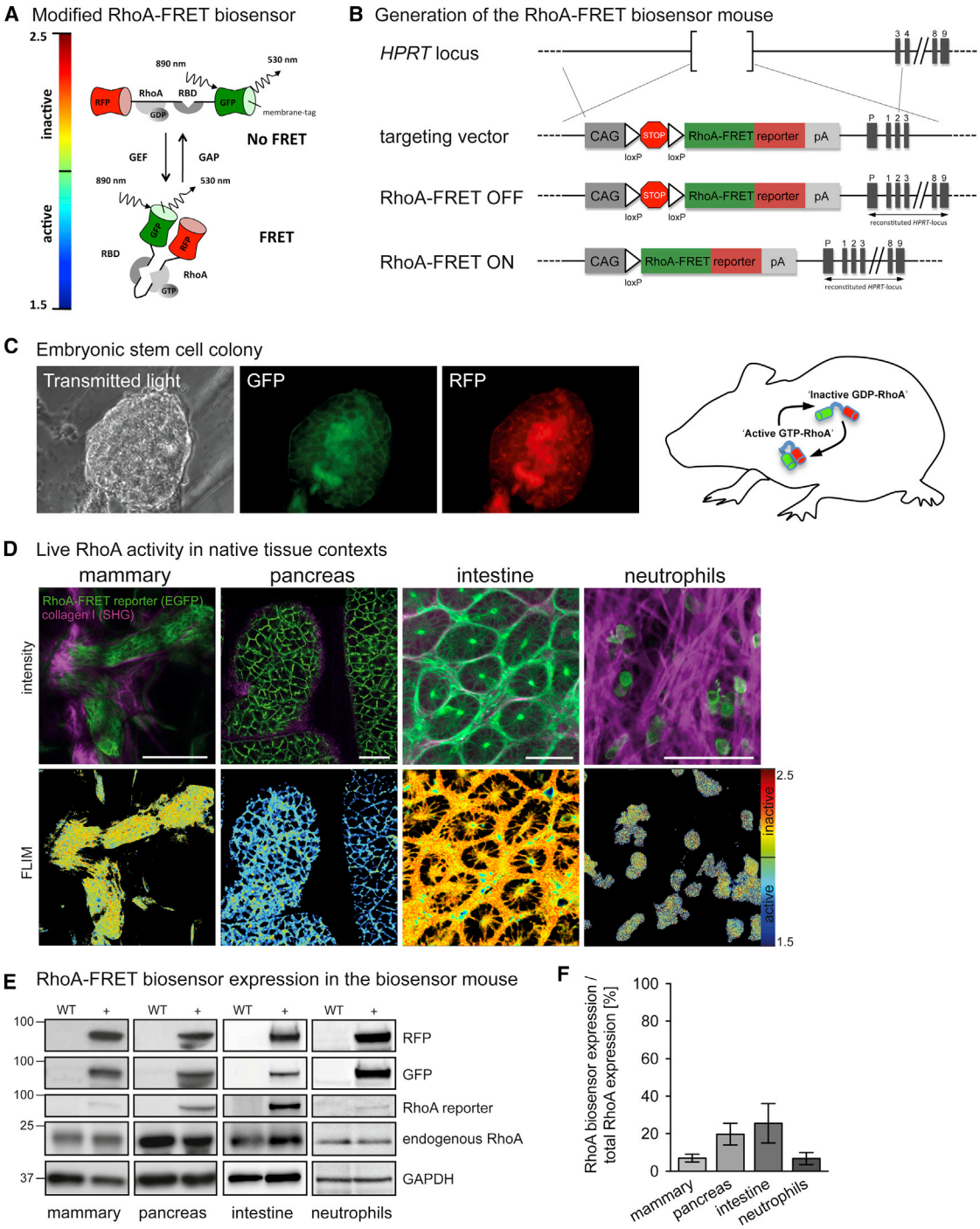

Figure 1. Generation of the RhoA-FRET Biosensor Mouse

(A and B) Schematic of the Raichu-RhoA biosensor (A), targeted to the *Hprt* locus to generate the RhoA-FRET biosensor mouse (B).

(C) Embryonic stem cell colony expressing the RhoA-FRET biosensor (GFP, green; RFP, red).

(D) RhoA activity in the mammary fat pad, pancreas, intestine, and neutrophils of RhoA-ON mice (RhoA-FRET biosensor, green; collagen-derived second harmonic generation (SHG) signal, magenta) with corresponding fluorescence lifetime (FLIM) images of RhoA activity (high RhoA activity, blue to green; low RhoA activity, yellow to red).

(E and F) Expression levels (E) and relative quantification (F) of the RhoA-FRET biosensor detected by immunoblot in different tissues of the RhoA-ON mouse (n = 3).

Columns, mean; bars, SEM. Scale bars, 50 μm.

Live subcellular RhoA activation in osteocyte processes during mechanical compression

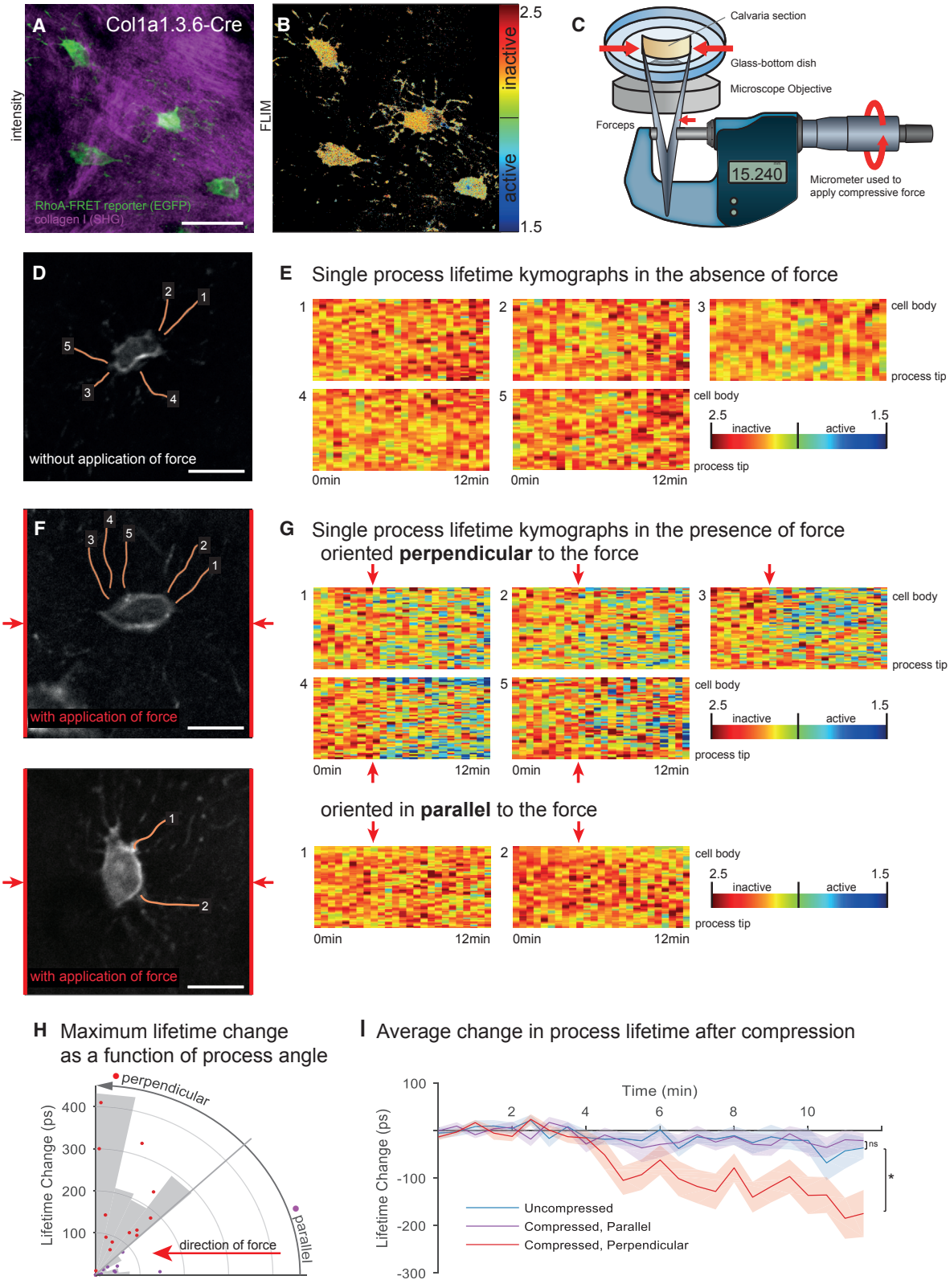

(legend on next page)

activity of RhoA along the length of individual protrusions, from the cell body to the process tip, over time, shown as kymographs (Figures 2D–2G, orange lines marking individual processes). In the absence of force, no changes in RhoA activity were observed in the osteocyte processes (Figure 2E). Upon the application of force (producing an ~1% lateral compression), an increase in RhoA activity was observed in a subpopulation of processes (Figure 2G, note change in lifetime post-compression, red arrows). Interestingly, this increase in RhoA activity was dependent on the directionality of the force being applied. Osteocyte processes aligned in parallel to the compressive force showed no significant change in RhoA activity, while processes closer to a perpendicular angle to the applied force demonstrated significant RhoA activation (Figures 2H and 2I). These data reveal orientation-dependent signaling events that lead to distinct subcellular RhoA activation in response to mechanical force transduction, and, therefore, they demonstrate a mechanosensing role of RhoA in bone. Manipulation of bone density and reciprocity to mechanical loading in diseases such as osteoporosis could, therefore, be assessed using this biosensor mouse in the context of therapeutic intervention.

Live Tracking of RhoA Activity in Swarming Neutrophils In Vivo

RhoA activity plays a vital role in cell migration. Here we demonstrate the ability of the RhoA-FRET biosensor mouse to characterize RhoA activity in highly motile cells, such as neutrophils. The use of primary neutrophils ex vivo is often hindered by their short viable lifetime, limiting the utility of transfection-based in vitro imaging studies (Basu et al., 2002). To investigate the regulation of RhoA activity during neutrophil swarming in vivo, we used LysozymeM-Cre (LysM-Cre) to drive expression of the RhoA-FRET biosensor (RhoA-OFF) in neutrophils. The ear was injected with inactivated *Staphylococcus aureus* bioparticles to enrich the local neutrophil population. We then laser ablated a resident dendritic cell (DC) to create a local site of tissue damage and, thus, a chemotactic gradient that attracts neutrophils (Figures 3A and 3B) (Hampton et al., 2015). Infiltrating neutrophils were imaged (Figure 3C; Movie S5, panels 2 and 3) and tracked over time (Figures 3D and 3E, black representing earlier time points and copper representing later time points; Movie S5, panel 4).

For each neutrophil, the RhoA activity from the front to the rear of the cell, relative to the direction of motion, was calculated and plotted as a kymograph of RhoA activity over time. This showed anterior and posterior fluctuations in RhoA activity as the neutrophils moved (Figure 3F). Following a methodology for in vitro tracking of Rac1 activity in neutrophils (Johnsson et al., 2014), the most active region of the cell was traced, illustrating oscillations of RhoA activity over time as neutrophils moved toward the site of tissue damage (Figure 3G, red line: rear, green line: front). Our in vivo readout of RhoA activity during neutrophil migration is consistent with previous work monitoring fluctuations of Rac1 activity in vitro during translocation and periodic stalling of primary neutrophils within chemotactic gradients (Johnsson et al., 2014). In addition, our data demonstrate that, upon reaching the site of injury in vivo, neutrophil remodelling of the damaged site occurs (Movie S5, panels 2 and 3 at ~15 min time post-swarming). We produced a large-scale kymograph of average RhoA activity of the swarming neutrophil population, as a function of the distance from the damaged site. This showed a gradual increase in RhoA activity based on the average activation level of the neutrophils present in the field of view, as well as collagen remodelling, as the collective cell population moved toward the site of damage upon inflammation (Figures 3H and 3I, collagen-remodelled zone within white dashed line). Similar analysis could be used to map the activity of individual or large populations of immune infiltrates or to monitor the deregulation of immune cell activity in disease settings, such as chronic wound healing (Kular et al., 2015) or immunotherapy in cancer (Steele et al., 2016).

Mammary RhoA Activity Cycles during Gestation and High RhoA Activity Is Co-opted in Invasive Breast Cancer

Recent investigations have revealed a key role of the small GTPase Rac1 in gestational involution (Akhtar et al., 2016). Similarily, downstream effectors of RhoA, such as PKN1, have been shown to play a role during the gestation cycle and lactation (Fischer et al., 2007). We therefore explored how RhoA signaling changed during both gestation-induced branching and development and in a cancer context. Expression of the RhoA-FRET biosensor (RhoA-OFF) was controlled by the mouse mammary tumor virus long terminal repeat (MMTV) driving Cre in the mammary epithelium. Carmine staining revealed no morphological defects at any stage of development (Figure 4A), and immunohistochemistry (IHC) for GFP and RFP confirmed RhoA-FRET biosensor expression (Figures 4B and 4C). FLIM analysis revealed decreasing RhoA activity during gestation, ranging from high levels in branching mammary ducts in virgin mice (blue in the FLIM maps) to a gradual decrease in activity in the alveoli

Figure 2. RhoA Activation in the Protrusions of Osteocytes Is Subject to Compressive Forces on the Bone and Is Dependent on the Angle of the Force Applied

(A and B) Osteocyte-specific expression of the RhoA-FRET biosensor (RhoA-OFF) (A, green) driven by Col1a1.3.6a-Cre in the calvaria with SHG signal (magenta) and associated FLIM images of RhoA activity (B).

(C) Compression apparatus.

(D–G) Time-lapse FLIM of RhoA activity in the osteocyte processes, with intensity images (D and F, tracked processes, red) and numbered and respective FLIM kymographs in the absence (E) and presence (G) of a compressive force applied after 5 min (red arrow).

(H) Maximum reduction in lifetime observed in each process during compression as a function of the angle of the process to the compressive force. Direction of the compressive force is indicated by the red arrow. Gray bars, weighted histogram of lifetime change; dots, individual processes parallel (purple) and perpendicular (red) to the compression force.

(I) Average change in fluorescence lifetime in osteocyte processes over the time course, quantified by the fifth percentile of the lifetime across the process (processes in uncompressed cells [blue, n = 15] and compressed cells parallel [purple, n = 18] and perpendicular [red, n = 13] to the force). Shaded area, SEM; *$p < 0.05$, by two-way ANOVA accounting for repeated measures. Scale bars, 25 μm.

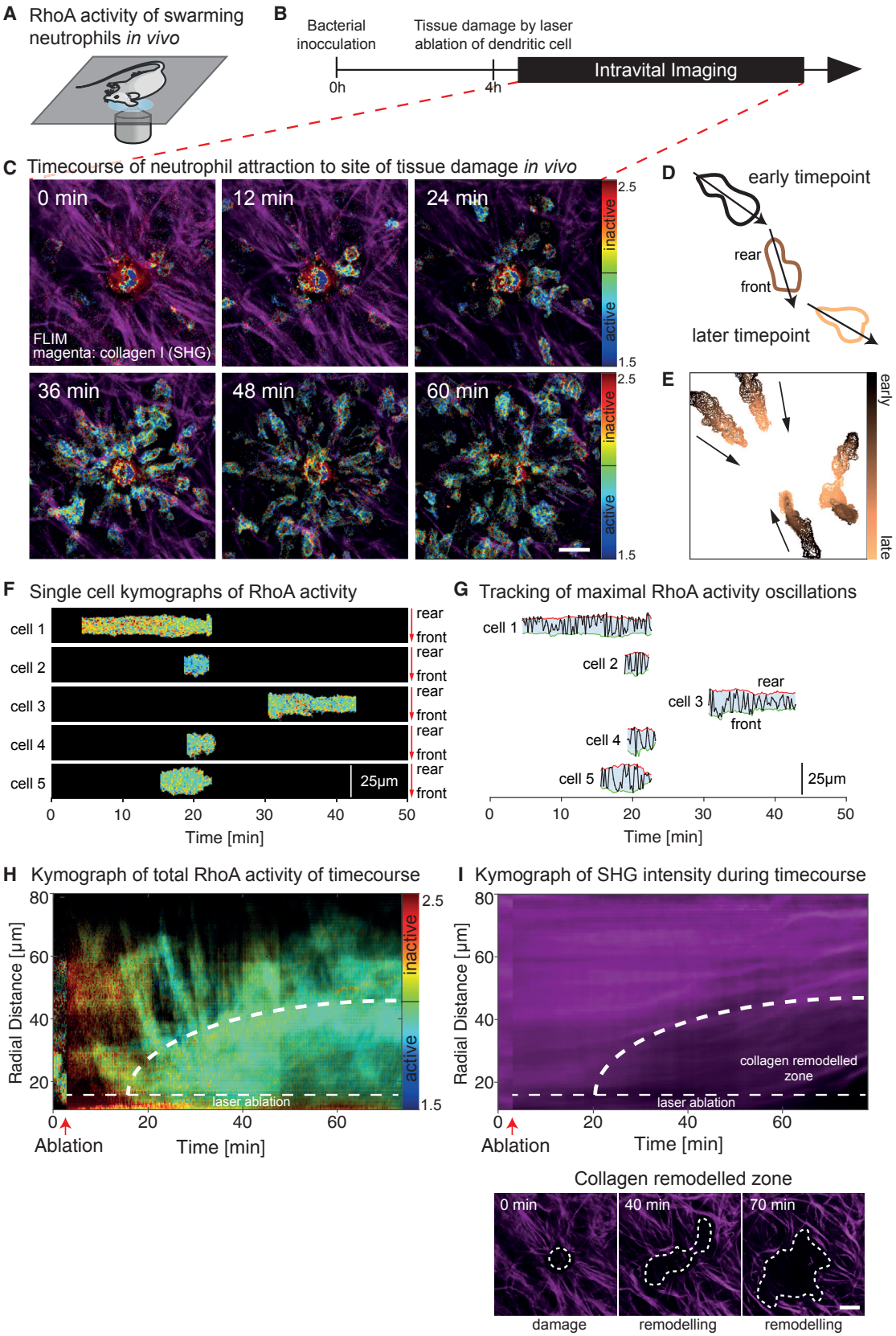

(legend on next page)

that form during pregnancy (Figures 4D and 4E; quantified in Figure 4F and Movie S6). RhoA became largely inactive in mature milk-producing alveoli during lactation and returned to an active state during mammary involution, which is triggered by weaning, when alveoli break down and the mammary tissue is remodelled to resemble virgin morphology (Figure 4E, fourth panel; quantified in Figure 4F). We then assessed RhoA activity in a cancerous setting using the polyoma middle-T antigen (PyMT) breast cancer model, driven by MMTV (Guy et al., 1992). Mice were imaged at 109 ± 2 days of age, when robust invasion and metastasis are known to occur (Lin et al., 2003). Comparing wild-type (WT) mammary glands to PyMT tissue, we observed a significant upregulation and co-option of RhoA activity in PyMT-induced tumors (Figure 4G), known to drive cell motility in invasive cancers. The RhoA biosensor mouse could, therefore, be used in various pre-clinical mouse models to examine emerging Rho GTPase targeting for the treatment of breast cancer (Rath and Olson, 2012).

Modulation of RhoA Activity during Pancreatic Cancer Progression and Metastasis

We have shown previously that RhoA is spatially regulated by mutant p53 in pancreatic ductal adenocarcinoma (PDAC) cells stably transfected with the RhoA-FRET biosensor, in an allograft approach (Timpson et al., 2011). To precisely model cancer progression in the context of the inherent pancreatic microenvironment, a GEM model of PDAC was used to examine RhoA activity over the course of native pancreatic cancer progression. The RhoA-OFF mouse was crossed to the Pdx1-Cre-driven KC (*KRas*$^{G12D/+}$ alone) and KPC (*KRas*$^{G12D/+}$ and *p53*$^{R172H/+}$) models of pancreatic cancer (Hingorani et al., 2003, 2005). In PDAC, *KRas*$^{G12D/+}$ and *p53*$^{R172H/+}$ are frequent oncogenic drivers, which accumulate during disease progression (Figure 5A). Both models have previously been shown to recapitulate the human disease histopathology (Biankin et al., 2012), and they display well-defined disease progression stages from precursor pancreatic intraepithelial neoplasia (PanINs) to fully developed invasive and metastatic PDAC, respectively.

Whole-body imaging confirmed that RhoA-FRET reporter expression could be detected locally in Pdx1-Cre mice, while, in highly metastatic KPC mice, it was readily observed at both primary and secondary sites (Figure 5B). Native pancreatic tissue displayed high RhoA activity (Figures 5C and 5D) that could be inhibited by the RhoA inhibitor C3-transferase (Figure 5E, left and middle panels; Figure 5F). Subsequent washout of the inhibitor and addition of an activator of RhoA, Calpeptin, reverted RhoA back to active levels (Figure 5E, right panel). This demonstrates the capability to monitor changes of RhoA activity both at the whole-organ and single-cell levels in situ, which we confirmed by glutathione S-transferase (GST) bead pull-down assays (Figure 5F).

Next, we assessed RhoA modulation in the progression of PDAC between ~150 and 250 days. In KC tumors, RhoA activity was progressively reduced from native pancreatic tissue, through the PanIN stages to fully developed PDAC (Figure 5G; Figure S6A). Similarly, in KPC mice, RhoA activity was decreased through consecutive PanIN stages to fully developed PDAC (Figure 5H; Figure S6B). We have previously shown that Src activity, which is known to play a key role in pancreatic cancer metastasis, was spatially regulated in subcutaneous PDAC tumors, with high activity at the invasive border (Morton et al., 2010; Nobis et al., 2013). We therefore sought to determine whether RhoA activity displayed a similar spatial pattern in KPC pancreatic tumors. At the final stage of PDAC progression, the tumor cortex showed elevated levels of RhoA activity compared to the center (Figure 5I). Furthermore, metastatic regions in the liver revealed higher levels of RhoA activity compared to the overall primary tumors (Figure 5J). This is consistent with previous observations that RhoA activity displays plasticity during tumor progression or invasion and requires switching of Rho GTPase activity for efficient metastasis (Byrne et al., 2016; Hirata et al., 2012; Huang et al., 2014; Sahai and Marshall, 2002; Timpson et al., 2011). We observed distinct spatial regulation of RhoA in PDAC progression, which could enhance our understanding of drug responses in vivo and help determine optimal Rho GTPase intervention strategies in this invasive disease (Conway et al., 2014; Rath and Olson, 2012; Rath et al., 2017; Vennin et al., 2017).

Longitudinal Monitoring of Drug Responses In Vivo Using Optical Windows Reveals Temporally Distinct Drug-Targeting Efficacies in Pancreatic and Breast Cancers

Accurate readouts of drug responses in vivo remains a primary challenge of pre-clinical testing of anti-cancer drugs (Amornphimoltham et al., 2011; Conway et al., 2014, 2017; Weissleder et al., 2016). Ex vivo imaging of excised tissue is limited to a

Figure 3. Neutrophil Swarming In Vivo Reveals Oscillation of RhoA Activity during Migration

(A and B) Intravital ear imaging in LysM-Cre; RhoA-OFF mice (A) and timeline of experiment to induce neutrophil infiltration (B). (A) was adapted from Servier Medial Art, licensed under the Creative Commons Attribution 3.0 Unported license (https://creativecommons.org/licenses/by/3.0/).

(C) Representative time series of neutrophil migration in vivo.

(D and E) Schematics (D) and tracking (E) of single neutrophils migrating toward the ablation (early time points, black; late time points, brown/orange).

(F) Kymographs of RhoA activity showing RhoA activity from the rear to the front of a selection of cells moving toward the damage site over time. This was computed by averaging spatially from the rear (top) to the front (bottom) of the cell, as determined by the direction of cell motion (shown in D). The y axis represents distance across the cell and the x axis represents time.

(G) Tracking of spatial position of the maximal RhoA activity from the rear (red) to the front (green) of the cells over time, illustrating oscillation in the location of maximum RhoA activity.

(H) Bulk kymograph of RhoA activity in the entire neutrophil population shown in the image as a function of distance from the damage zone and averaged over the image (weighted by fluorescence intensity).

(I) Upper panel: kymograph of the associated SHG intensity in the damaged area, reading out density of cross-linked collagen, as a function of distance from the damage zone and time, revealing collagen remodelling and clearance near the damage zone that results in a loss of SHG signal (highlighted by dashed white line). Lower panel: individual SHG images at a number of time points are shown. Scale bars, 25 μm.

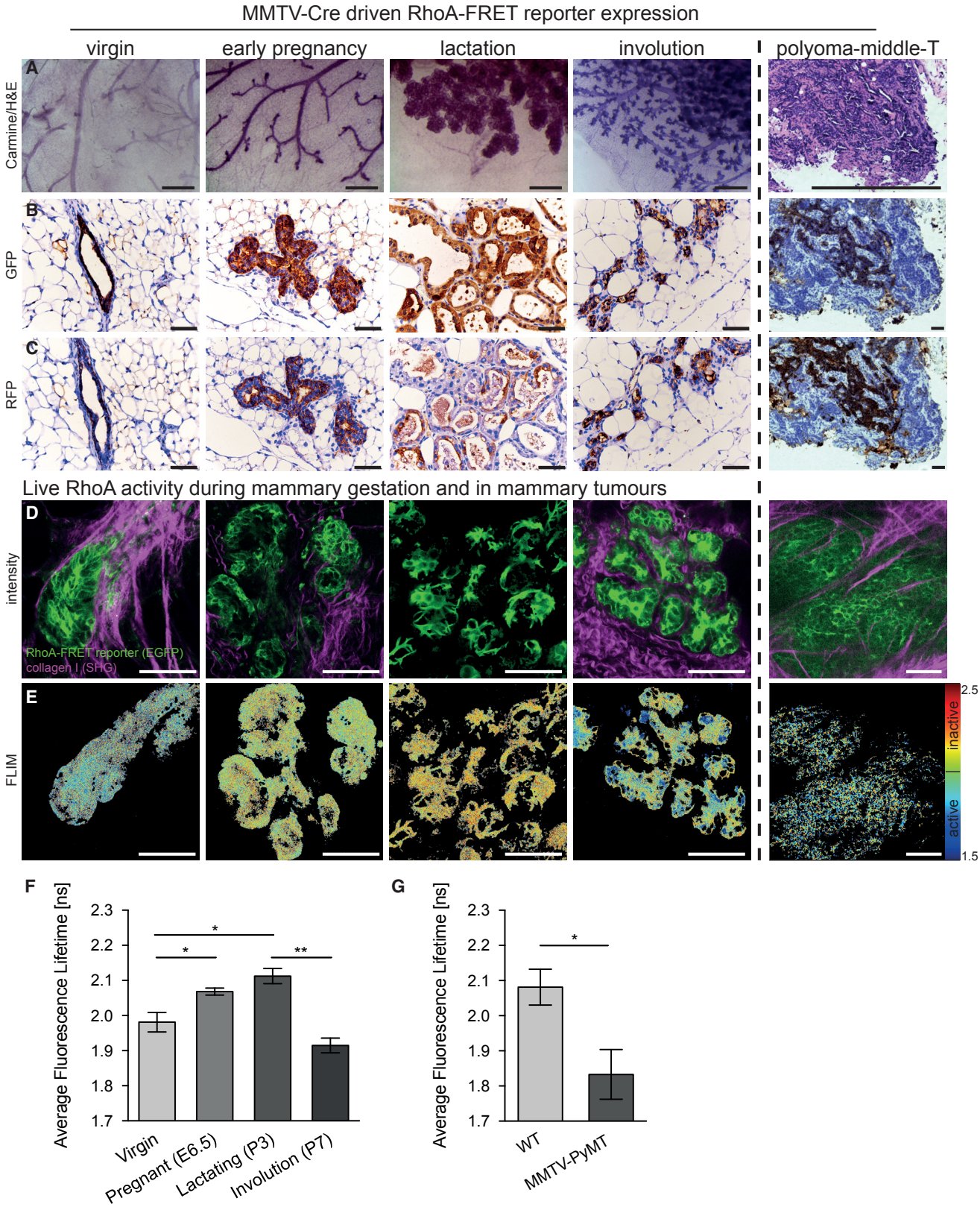

(legend on next page)

single time point, and comparison of different animals across time points constitutes a source of significant biological noise in the readout of drug-targeting efficacy. To monitor changes in RhoA activity in the same mouse over time and improve the fidelity of drug readouts, we used surgical implantation of abdominal imaging windows (AIWs) and mammary imaging windows (MIWs) for pancreatic and breast cancer drug-targeting studies, respectively (Figure 6) (Gligorijevic et al., 2009; Ritsma et al., 2012, 2013, 2014).

Mice were allowed to develop primary KPC tumors over a period of 125 ± 22 days, prior to surgical engraftment with AIWs to allow for intravital PDAC imaging in the abdominal cavity (Figures 6A and 6B). Here we used erlotinib, a second-generation epidermal growth factor receptor (EGFR) inhibitor, administered in three daily consecutive gavages to mice with developed primary KPC tumors (Figure 6C). RhoA is often associated with enhanced migration of cancer cells and is a downstream effector of EGFR, which is itself a potential therapeutic target (Ardito et al., 2012; Navas et al., 2012). Therefore, as a proof of principle, RhoA activity was tracked over 24 hr in PDAC after erlotinib administration. Here, robust inhibition was evident at 3 hr after the final administration, which subequently returned to baseline levels after 24 hr (Figures 6D and 6E).

Similarly, oral gavaging with dasatinib, an Src/Abl kinase inhibitor that is currently under clinical investigation as an anti-invasive in PDAC (Evans et al., 2012), revealed that dasatinib-based indirect inhibition of RhoA was maximal after 7 hr and was no longer observed after 24 hr (Figures 6F and 6G). This real-time imaging approach represents a fundamental advance in single-cell drug target validation to optimize in vivo scheduling for maximum benefit (Dubach et al., 2017; Vennin et al., 2017).

Having demonstrated that RhoA activity was upregulated in PyMT-driven mammary carcinomas (Figure 4G), PyMT mice expressing the RhoA-FRET reporter were allowed to develop primary tumors for up to 86 ± 14 days. MIWs were then surgically implanted on top of the developed tumors to track drug response in vivo in a mammary tumor context (Figures 6H–6J; Movie S6). Subsequent FLIM measurement of RhoA activity allowed us to observe effective inhibition following 2–6 hr of dasatinib administration, which after 24 hr reverted to control levels (Figures 6K and 6L).

Finally, spatial regulation of RhoA was assessed in intestinal crypts using AIWs (Figures 7A–7C). A gradient of RhoA activity along the crypt-villus axis was observed with maximal activity at the crypt base, decreasing to basal levels at approximately 30 μm (Figures 7C–7E; Figure S7; Movie S7). This suggests a site-specific role for RhoA signaling in the stem cell compartment of small intestinal crypts in vivo (Figures 7D and 7E), consistent with our previous work assessing Rac1 activity in this setting (Johnsson et al., 2014; Myant et al., 2013). The stem cell compartment is often a site of progenitor hyperproliferation and transformation (Ritsma et al., 2014), and, therefore, Rho GTPase targeting could be differentially traced in this site-specific setting and highlights another advantage of the RhoA-FRET mouse.

Here, we have demonstrated that longitudinal in vivo imaging using FLIM-FRET through optical windows allows for accurate monitoring of RhoA and its inhibition in primary tissue or tumors over time. Detailed knowledge of how specific inhibitors fare in pre-clinical in vivo settings will allow for the tailoring of more precisely timed treatment regimens, resulting in the most effective treatment achievable with each compound.

DISCUSSION

We have described the development of a RhoA-FRET mouse that ubiquitously (RhoA-ON) or conditionally (RhoA-OFF) expresses a RhoA-FRET biosensor from the *Hprt* locus in a variety of tissues. The *Hprt* locus was chosen in this study for its uniformly low level of expression, balancing the need for a high signal-to-noise ratio for intravital FLIM-FRET imaging while avoiding possible dominant-negative effects caused by excessive overexpression of the biosensor (Erami et al., 2016; Goto et al., 2013; Johnsson et al., 2014). A modified version of the intra-molecular Raichu-RhoA reporter containing the EGFP/mRFP fluorophore pair was used in place of ECFP/YPet (Yoshizaki et al., 2003) to avoid potential problems with recombination from tandem repeats of related fluorescent protein sequences during mouse generation (Komatsubara et al., 2015).

The RhoA biosensor used in this study reports on the regulation of RhoA activity by GEF/GAPs in native tissue using the Raichu design. We note that a range of biosensors provide the ability to read out distinct aspects of RhoA activity (Fritz et al., 2013; Kardash et al., 2010; Pertz et al., 2006; van Unen et al., 2015; Yang et al., 2016). Converting other key biosensors to similar in vivo applications, such as the cytoplasmic DORA sensors with RhoA binding to a PKN1 domain (van Unen et al., 2015) or the RhoA-2G biosensor that can report on GDI activity (Fritz et al., 2013; Pertz et al., 2006), will collectively allow us to test multiple intricate and subtle changes in upstream and downstream cascades of this vital molecular switch.

To characterize our RhoA-FRET biosensor mouse in more detail, we first examined the regulation of RhoA in normal tissues prior to disease contexts. Tracking RhoA activity in real time during mechanosensing of osteocytes, during migration events of neutrophils, or during mammary gestation revealed the potential of the RhoA-FRET biosensor mouse for the dynamic study of RhoA activity in healthy and disease states, which is difficult to access using biochemical methods in tissues and in cells with intricate spatiotemporal and subcellular signaling events

Figure 4. Mammary Tissue Displays Differential RhoA Activity during Gestation and in PyMT-Driven Cancer

(A–C) Carmine and H&E stains (A), GFP (B), and RFP (C) IHC of different stages of gestation (5-week-old virgin, day 6.5 of pregnancy, postnatal day 3 for lactation, day 4 of involution, and 109 ± 2 days for PyMT tumors). Scale bars, 500 μm (A) and 50 μm (B and C).

(D–G) Imaging of RhoA activity during gestation and in PyMT-driven breast cancer. RhoA-OFF mice crossed to MMTV-Cre (D, RhoA-FRET biosensor, green; collagen-derived SHG signal, magenta) with associated FLIM images (E) and quantification of RhoA activity during gestation (F) and PyMT-driven cancer formation (G). n = 3 mice per condition, 690 cells in total.

Columns, mean; bars, SEM; *p < 0.05 and **p < 0.01 by unpaired Student's t test. Scale bars, 50 μm.

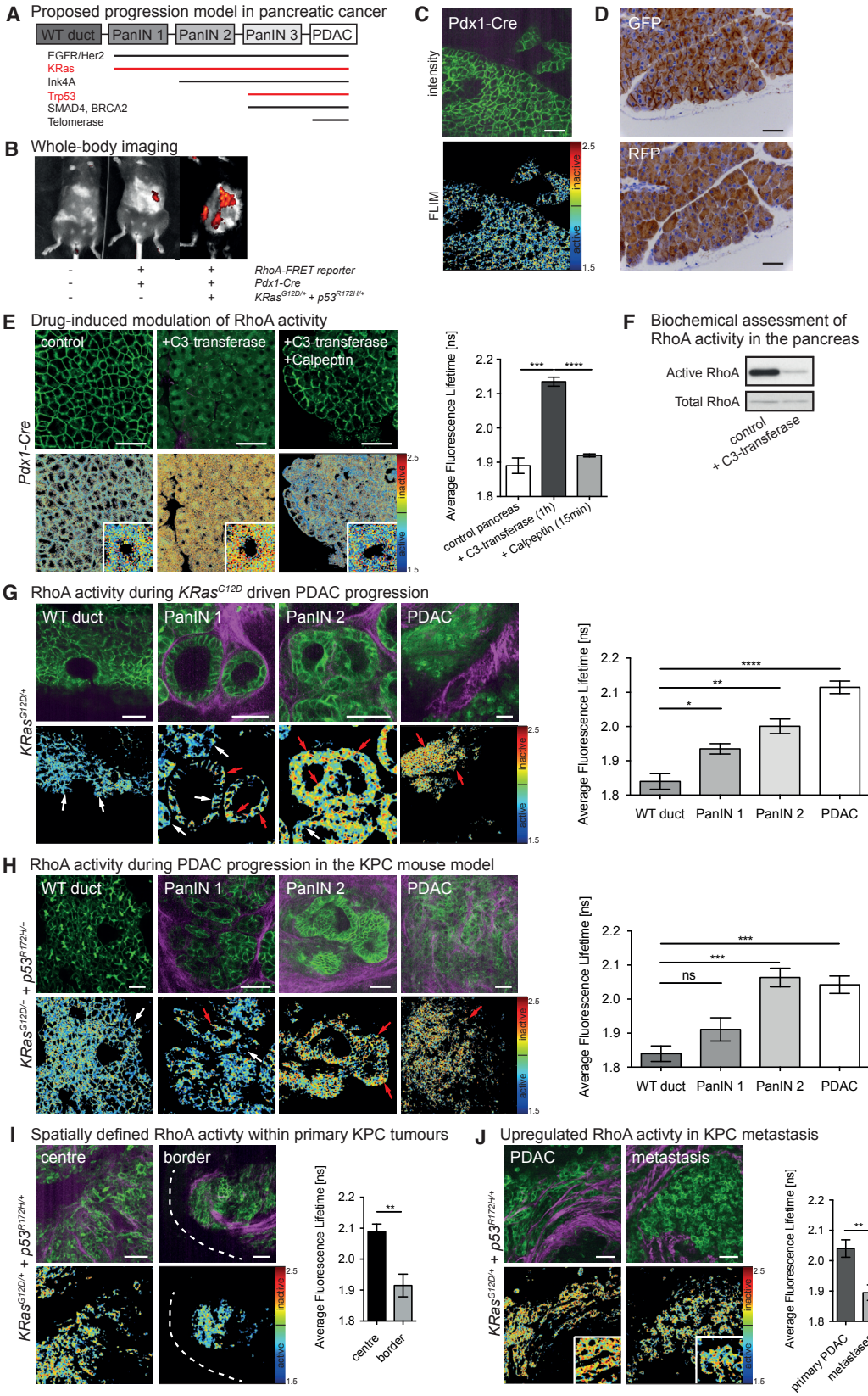

(legend on next page)

governing regulation. We imaged osteocytes in their native bone matrix to investigate the role of subcellular RhoA signaling in mechanotransduction. Here, we revealed that the level of RhoA activation in the dendritic processes varies strongly depending on the angle of the process with respect to the force. This suggests that the dendritic processes of osteocytes may function as mechanotransducers of shear forces following stress in the fluid-filled lacunae containing the dendritic processes (Burra et al., 2010; Thi et al., 2013). Furthermore, it has been demonstrated that lacunae perpendicular to compression experienced more microdamage than those aligned in parallel (Prendergast and Huiskes, 1996), potentially resulting in enhanced signal transduction. This demonstrates the utility of the RhoA-FRET mouse in subcellular intravital imaging studies of mechanical loading and disorders of bone remodelling.

The rapid gain in immunotherapy applications in melanoma (Drake et al., 2014) and other cancers could also benefit from our capacity to monitor immune infiltration at a subcellular level in real time (Cooper et al., 2016). In this study, we mapped the population dynamics of RhoA activity during neutrophil infiltration to sites of local damage in vivo. The observed oscillations in RhoA activity during in vivo migration were similar to the oscillations in Rac1 activity in neutrophil migration during in vitro chemotaxis (Johnsson et al., 2014), further undermining the crosstalk of these small GTPases in the coordinated migration of neutrophils. Recent work in pancreatic cancer has emphasized the role of tumor-associated neutrophils in metastatic pancreatic cancer progression, where neutrophil depletion via CXCR2 inhibition improved T cell infilration and immunotherapy performance (Steele et al., 2016). Future adaptation of our neutrophil-swarming analysis could, therefore, be used to allow for fine-tuned targeting of immune checkpoint inhibiton in this and other cancer types (Steele et al., 2016).

We next examined RhoA regulation during distinct stages of mammary tissue gestation, in line with recent investigations of the role of Rac1 in these processes (Akhtar et al., 2016) and the described crosstalk between both Rac1 and RhoA in normal tissue and cancer progression (Sahai and Marshall, 2002). Here we observed inactivation of RhoA over the course of pregnancy up to lactation, when the lactating alveoli are sealed by tight junctions. In contrast, we observed activation of RhoA during involution of the mammary gland, when tissue is extensively remodelled. We also found a co-option of RhoA activity in a mouse model of invasive and metastatic breast cancer. Similarly, in line with recent investigations on the action of the upstream regulator RhoA GEF-H1 (Cullis et al., 2014), we observed a spatial upregulation of RhoA in mouse models of PDAC progression. These studies emphasize the advantage of genetically encoded FRET biosensor mice, which can be crossed to GEM cancer models to readily quantify protein activity in situ while tumors form, progress, and metastasize in their intact microenvironment.

Having shown that RhoA activity can be co-opted in invasive and metastatic mammary and pancreatic carcinomas, we used the RhoA-FRET mouse to directly visualize the inhibition of RhoA using small molecule inhibitors. We use optical windows to longitudinally read out RhoA response to treatment, illustrating the value of the mouse in optimizing preclinical drug targeting in native tissue microenvironments (Conway et al., 2014). In the KPC mice, it was observed that dasatinib-induced RhoA inhibition was delayed relative to the PyMT breast cancer model. This may reflect organ-specific bioavailability of the drug or the known difficulty of drug delivery in pancreatic cancer (Neesse et al., 2013), demonstrating the importance of drug target validation in disease or organ-specific contexts. Moreover, examining the intra-tumoral heterogeneity of drug response to treatment could also be investigated in this mouse, exploiting the high spatial resolution provided by intravital microscopy for both primary and secondary sites, while tracking non-responsive subpopulations over time could help understand the development of resistance in vivo, which is currently poorly understood in many disease areas.

Lastly, the in vivo distribution, regulation, as well as potential redundancy of upstream or downstream regulators of RhoA, such as GEFs, GAPs, and GDIs, could also be investigated in multiple organ and disease settings (Cerikan et al., 2016; Cherfils and Zeghouf, 2013; Porter et al., 2016). This could help dissect, in real time, the complex changes that occur during disease progression, which, in many cases, do not involve loss or gain of RhoA activity but rather transient modulation of this vital molecular switch.

EXPERIMENTAL PROCEDURES

Animals

Animals were kept in conventional animal facilities. All experiments were carried out in compliance with guidelines of the UK Home Office, the Australian code of practice for the care and use of animals for scientific purposes, and the Garvan Ethics Committee. Mice were kept on a 12-hr day-night cycle and fed ad libitum.

Drug Treatments

Dasatinib was administered by oral gavage at 10 mg/kg in 80 mmol/L citrate buffer for three consecutive days before imaging. Erlotinib was administered

Figure 5. RhoA Activity in KPC Tumors Is Upregulated at the Invasive Border and in Liver Metastases

(A) Progression of pancreatic ductal adenocarcinoma (PDAC) via pancreatic intraepithelial neoplasms (PanINs), with reported key drivers highlighting mutant *KRas* and mutant *Trp53* (red) used in the KPC mouse model (adapted from Bardeesy and DePinho, 2002).

(B) Whole-body imaging of the RhoA-FRET biosensor (WT, Pdx1-Cre, and KPC).

(C and D) RhoA-FRET biosensor expression (RhoA-OFF) in the pancreas driven by Pdx1-Cre (C) and GFP and RFP IHC (D).

(E) Decreased RhoA activity upon C3-transferase treatment, followed by Calpeptin-mediated re-activation of RhoA. n = 3 mice per treatment group, 225 cells.

(F) Pancreatic RhoA activity measured by GST-Rhotekin-RBD pull-down.

(G) RhoA activity during KC ($KRas^{G12D/+}$) tumor progression. n $\geq$ 3 mice per stage, 244 cells.

(H) RhoA activity during KPC ($KRas^{G12D/+}$ + $p53^{R172H/+}$) tumor progression (white arrows, active cells; red arrows, inactive cells). n = 3 mice per tumor stage, 355 cells.

(I and J) Quantification of RhoA activity in late-stage KPC tumor center versus border (I, n = 4 mice, 168 cells) and liver metastases (J, n = 5 mice, 134 cells). Columns, mean; bars, SEM; *p < 0.05, **p < 0.01, ***p < 0.001, and ****p < 0.001 by unpaired Student's t test. Scale bars, 50 μm.

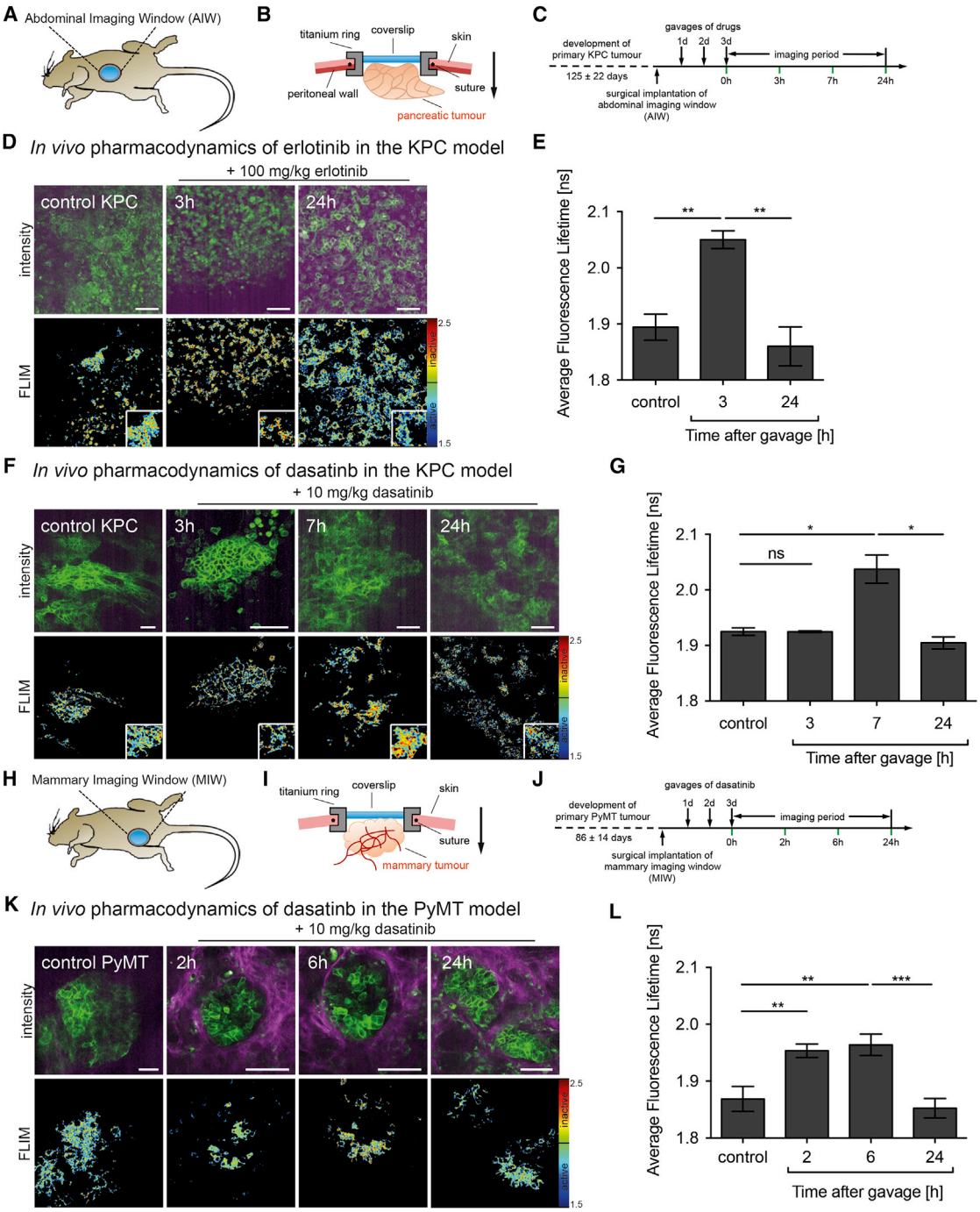

Figure 6. RhoA Activity in KPC and PyMT Tumors In Vivo Imaged through Optical Imaging Windows

(A) Schematic of an abdominal imaging window (AIW) implanted into a mouse.

(B) In vivo imaging of a late-stage KPC tumor through an AIW.

(C) Timeline of AIW surgery, subsequent drug treatment regimen, and imaging time points.

(D and E) Live time course (D) and quantification of RhoA activity (E) after 3 daily oral gavages of 100 mg/kg erlotinib in vivo in KPC tumors, showing effective RhoA inhibition after 3 hr. n = 3 mice, 90 cells.

(F and G) Live time course (F) and quantification of RhoA activity (G) after 3 daily oral gavages of 10 mg/kg dasatinib in vivo in KPC tumors, showing effective RhoA inhibition after 7 hr. n = 3 mice, 291 cells.

(H and I) Schematics of a mammary imaging window (MIW) implanted into a mouse (H) on top of a late-stage PyMT-driven mammary tumor (I).

(legend continued on next page)

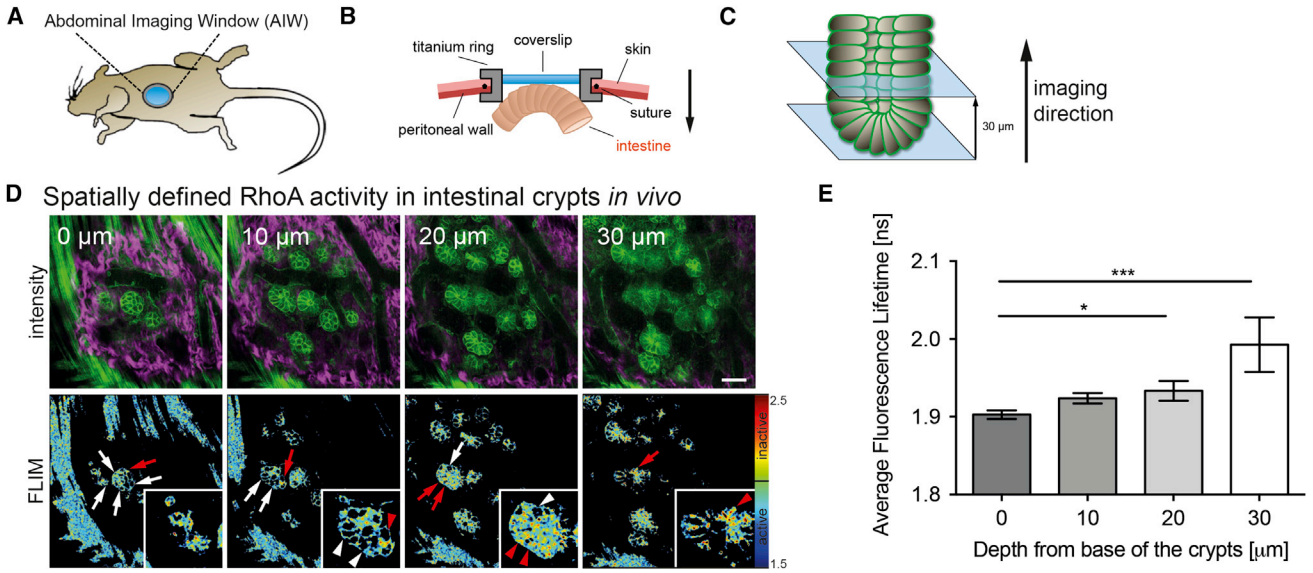

Figure 7. Spatially Defined RhoA Activity in the Small Intestine In Vivo Imaged through Optical Imaging Windows

(A–C) Schematics of AIW imaging of the small intestine (A and B) and direction of imaging from the base of the crypts toward the villi (C).

(D and E) In vivo imaging (D) and quantification of RhoA activity (E) in crypts of the duodenum, revealing spatially distinct RhoA inactivation with progression away from the base of the crypts (white arrows, active cells; red arrows, inactive cells). n = 3, 12 crypts, 255 cells.

Columns, mean; bars, SEM; *p < 0.05 and ***p < 0.001 by unpaired Student's t test. Scale bars, 50 μm.

by single gavage at 100 mg/kg in 0.5% w/v methyl cellulose. C3-transferase was used at 0.5 μg/mL and Calpeptin at 0.2 U/mL on ex-vivo-imaged pancreas.

FLIM-FRET Imaging of RhoA-FRET Biosensor

FLIM-FRET measurements were conducted using a Titanium:Sapphire femtosecond pulsed laser and time-correlated single-photon-counting (TCSPC) equipment. Data were analyzed using LaVision Impector, phasor analysis with TTTR data analysis software, and FLIMfit.

See the Supplemental Experimental Procedures for more details.

SUPPLEMENTAL INFORMATION

Supplemental Information includes Supplemental Experimental Procedures, seven figures, and seven movies and can be found with this article online at https://doi.org/10.1016/j.celrep.2017.09.022.

AUTHOR CONTRIBUTIONS

Data Acquisition, M.N., D.H., S.C.W., S.K., D. Stevenson, W.L., M.C.L., M.K., N.R., C.V., A.B., A.Z., J.R.W.C., A.M.L., D.G.-O., S.N.W., J.M.W.Q., J.P.S., L.Z., A. Mrowinska, A. Masedunskas, G.d.M.-N., M.P., and E.J.M.; Conception, Design, and Funding, M.N., D.H., S.C.W., S.K., C.J.O., S.T.G., P.A.B., P.I.C., H.H., E.C.H., P.W.G., R.P.H., A.-K.E.J., H.C.E.W., O.J.S., J.P.M., D. Strathdee, K.I.A., and P.T.; Methodology, M.N., D.H., S.C.W., A.B., J.B., T.C., K.I.A., and P.T.; Data Analysis and Interpretation, M.N., D.H., S.C.W., S.K., D.G.-O., A. Magenau, J.P.M., M.S.S., K.I.A., and P.T.; Manuscript Writing and Revision, M.N., D.H., S.C.W., K.I.A., and P.T.

ACKNOWLEDGMENTS

The authors thank Dr. Haley Bennett, Dr. Andrew Burgess, Dr. David Croucher, and Kendelle Murphy for critical reading of the manuscript. P.T., M.N., D.H., S.C.W., M.K., M.C.L., W.L., N.R., C.V., J.R.W.C., and A. Magenau were funded by NHMRC project grants (1043501, 1089497, 1105640, and 1129401), ARC Future (FT120100880) and Len Ainsworth Pancreatic Cancer Fellowships, the Cancer Council NSW (RG 14-08), Sydney Catalyst, and Tour de Cure. K.I.A., M.N., E.J.M., A. Mrowinska, S.K., J.P.S., D. Strathdee, D. Stevenson, O.J.S., and J.P.M. were funded by a CRUK core grant. We thank R.T. Hall for histology funding and the IMCF at BIOCEV, an institution supported by the MEYS CR (LM2015062 Czech-BioImaging), for their support with FLIM data analysis.

Received: April 27, 2017
Revised: July 6, 2017
Accepted: September 5, 2017
Published: October 3, 2017

REFERENCES

Akhtar, N., Li, W., Mironov, A., and Streuli, C.H. (2016). Rac1 Controls Both the Secretory Function of the Mammary Gland and Its Remodeling for Successive Gestations. Dev. Cell *38*, 522–535.

Amornphimoltham, P., Masedunskas, A., and Weigert, R. (2011). Intravital microscopy as a tool to study drug delivery in preclinical studies. Adv. Drug Deliv. Rev. *63*, 119–128.

Ardito, C.M., Grüner, B.M., Takeuchi, K.K., Lubeseder-Martellato, C., Teichmann, N., Mazur, P.K., Delgiorno, K.E., Carpenter, E.S., Halbrook, C.J., Hall,

(J) Timeline of MIW surgery, drug treatment regimen, and imaging time points.

(K and L) Live time course (K) and quantification of RhoA activity (L) after 3 daily oral gavages of 10 mg/kg dasatinib in vivo in a PyMT tumor, showing effective inhibition of RhoA after 2 hr. n = 1, 100 cells.

Columns, mean; bars, SEM; *p < 0.05, **p < 0.01, and ***p < 0.001 by unpaired Student's t test. Scale bars, 50 μm.

J.C., et al. (2012). EGF receptor is required for KRAS-induced pancreatic tumorigenesis. Cancer Cell *22*, 304–317.

Bardeesy, N., and DePinho, R.A. (2002). Pancreatic cancer biology and genetics. Nat. Rev. Cancer *2*, 897–909.

Basu, S., Hodgson, G., Katz, M., and Dunn, A.R. (2002). Evaluation of role of G-CSF in the production, survival, and release of neutrophils from bone marrow into circulation. Blood *100*, 854–861.

Biankin, A.V., Waddell, N., Kassahn, K.S., Gingras, M.-C., Muthuswamy, L.B., Johns, A.L., Miller, D.K., Wilson, P.J., Patch, A.-M., Wu, J., et al.; Australian Pancreatic Cancer Genome Initiative (2012). Pancreatic cancer genomes reveal aberrations in axon guidance pathway genes. Nature *491*, 399–405.

Bishop, A.L., and Hall, A. (2000). Rho GTPases and their effector proteins. Biochem. J. *348*, 241–255.

Braga, V.M., Machesky, L.M., Hall, A., and Hotchin, N.A. (1997). The small GTPases Rho and Rac are required for the establishment of cadherin-dependent cell-cell contacts. J. Cell Biol. *137*, 1421–1431.

Burra, S., Nicolella, D.P., Francis, W.L., Freitas, C.J., Mueschke, N.J., Poole, K., and Jiang, J.X. (2010). Dendritic processes of osteocytes are mechanotransducers that induce the opening of hemichannels. Proc. Natl. Acad. Sci. USA *107*, 13648–13653.

Byrne, K.M., Monsefi, N., Dawson, J.C., Degasperi, A., Bukowski-Wills, J.C., Volinsky, N., Dobrzyński, M., Birtwistle, M.R., Tsyganov, M.A., Kiyatkin, A., et al. (2016). Bistability in the Rac1, PAK, and RhoA Signaling Network Drives Actin Cytoskeleton Dynamics and Cell Motility Switches. Cell Syst. *2*, 38–48.

Cerikan, B., Shaheen, R., Colo, G.P., Gläßer, C., Hata, S., Knobeloch, K.-P., Alkuraya, F.S., Fässler, R., and Schiebel, E. (2016). Cell-Intrinsic Adaptation Arising from Chronic Ablation of a Key Rho GTPase Regulator. Dev. Cell *39*, 28–43.

Cherfils, J., and Zeghouf, M. (2013). Regulation of small GTPases by GEFs, GAPs, and GDIs. Physiol. Rev. *93*, 269–309.

Conway, J.R.W., Carragher, N.O., and Timpson, P. (2014). Developments in preclinical cancer imaging: innovating the discovery of therapeutics. Nat. Rev. Cancer *14*, 314–328.

Conway, J.R.W., Warren, S.C., and Timpson, P. (2017). Context-dependent intravital imaging of therapeutic response using intramolecular FRET biosensors. Methods *128*, 78–94.

Cooper, Z.A., Reuben, A., Spencer, C.N., Prieto, P.A., Austin-Breneman, J.L., Jiang, H., Haymaker, C., Gopalakrishnan, V., Tetzlaff, M.T., Frederick, D.T., et al. (2016). Distinct clinical patterns and immune infiltrates are observed at time of progression on targeted therapy versus immune checkpoint blockade for melanoma. OncoImmunology *5*, e1136044.

Cullis, J., Meiri, D., Sandi, M.J., Radulovich, N., Kent, O.A., Medrano, M., Mokady, D., Normand, J., Larose, J., Marcotte, R., et al. (2014). The RhoGEF GEF-H1 is required for oncogenic RAS signaling via KSR-1. Cancer Cell *25*, 181–195.

Drake, C.G., Lipson, E.J., and Brahmer, J.R. (2014). Breathing new life into immunotherapy: review of melanoma, lung and kidney cancer. Nat. Rev. Clin. Oncol. *11*, 24–37.

Dubach, J.M., Kim, E., Yang, K., Cuccarese, M., Giedt, R.J., Meimetis, L.G., Vinegoni, C., and Weissleder, R. (2017). Quantitating drug-target engagement in single cells in vitro and in vivo. Nat. Chem. Biol. *13*, 168–173.

Erami, Z., Herrmann, D., Warren, S.C., Nobis, M., McGhee, E.J., Lucas, M.C., Leung, W., Reischmann, N., Mrowinska, A., Schwarz, J.P., et al. (2016). Intravital FRAP imaging using an E-cadherin-GFP mouse reveals disease- and drug-dependent dynamic regulation of cell-cell junctions in live tissue. Cell Rep. *14*, 152–167.

Evans, T.R.J., Van Cutsem, E., Moore, M.J., Purvis, J.D., Strauss, L.C., Rock, E.P., Lee, J., Lin, C., Rosemurgy, A., Arena, F.P., et al. (2012). Dasatinib combined with gemcitabine (Gem) in patients (pts) with locally advanced pancreatic adenocarcinoma (PaCa): design of CA180-375, a placebo-controlled, randomized, double-blind phase II trial. J. Clin. Oncol. *30* (*Suppl 15*), TPS4134.

Fischer, A., Stuckas, H., Gluth, M., Russell, T.D., Rudolph, M.C., Beeman, N.E., Bachmann, S., Umemura, S., Ohashi, Y., Neville, M.C., and Theuring, F. (2007). Impaired tight junction sealing and precocious involution in mammary glands of PKN1 transgenic mice. J. Cell Sci. *120*, 2272–2283.

Friedl, P., and Alexander, S. (2011). Cancer invasion and the microenvironment: plasticity and reciprocity. Cell *147*, 992–1009.

Fritz, R.D., Letzelter, M., Reimann, A., Martin, K., Fusco, L., Ritsma, L., Ponsioen, B., Fluri, E., Schulte-Merker, S., van Rheenen, J., and Pertz, O. (2013). A versatile toolkit to produce sensitive FRET biosensors to visualize signaling in time and space. Sci. Signal. *6*, rs12.

Gligorijevic, B., Kedrin, D., Segall, J.E., Condeelis, J., and van Rheenen, J. (2009). Dendra2 photoswitching through the Mammary Imaging Window. J. Vis. Exp. (*28*), 1278.

Goto, A., Sumiyama, K., Kamioka, Y., Nakasyo, E., Ito, K., Iwasaki, M., Enomoto, H., and Matsuda, M. (2013). GDNF and endothelin 3 regulate migration of enteric neural crest-derived cells via protein kinase A and Rac1. J. Neurosci. *33*, 4901–4912.

Guy, C.T., Cardiff, R.D., and Muller, W.J. (1992). Induction of mammary tumors by expression of polyomavirus middle T oncogene: a transgenic mouse model for metastatic disease. Mol. Cell. Biol. *12*, 954–961.

Hall, A., and Nobes, C.D. (2000). Rho GTPases: molecular switches that control the organization and dynamics of the actin cytoskeleton. Philos. Trans. R. Soc. Lond. B Biol. Sci. *355*, 965–970.

Hamamura, K., Swarnkar, G., Tanjung, N., Cho, E., Li, J., Na, S., and Yokota, H. (2012). RhoA-mediated signaling in mechanotransduction of osteoblasts. Connect. Tissue Res. *53*, 398–406.

Hampton, H.R., Bailey, J., Tomura, M., Brink, R., and Chtanova, T. (2015). Microbe-dependent lymphatic migration of neutrophils modulates lymphocyte proliferation in lymph nodes. Nat. Commun. *6*, 7139.

Heasman, S.J., Carlin, L.M., Cox, S., Ng, T., and Ridley, A.J. (2010). Coordinated RhoA signaling at the leading edge and uropod is required for T cell transendothelial migration. J. Cell Biol. *190*, 553–563.

Hetmanski, J.H.R., Schwartz, J.-M., and Caswell, P.T. (2016). Rationalizing Rac1 and RhoA GTPase signaling: a mathematical approach. Small GTPases *Aug 30*, 1–6.

Hingorani, S.R., Petricoin, E.F., Maitra, A., Rajapakse, V., King, C., Jacobetz, M.A., Ross, S., Conrads, T.P., Veenstra, T.D., Hitt, B.A., et al. (2003). Preinvasive and invasive ductal pancreatic cancer and its early detection in the mouse. Cancer Cell *4*, 437–450.

Hingorani, S.R., Wang, L., Multani, A.S., Combs, C., Deramaudt, T.B., Hruban, R.H., Rustgi, A.K., Chang, S., and Tuveson, D.A. (2005). Trp53R172H and KrasG12D cooperate to promote chromosomal instability and widely metastatic pancreatic ductal adenocarcinoma in mice. Cancer Cell *7*, 469–483.

Hirata, E., Yukinaga, H., Kamioka, Y., Arakawa, Y., Miyamoto, S., Okada, T., Sahai, E., and Matsuda, M. (2012). In vivo fluorescence resonance energy transfer imaging reveals differential activation of Rho-family GTPases in glioblastoma cell invasion. J. Cell Sci. *125*, 858–868.

Huang, B., Lu, M., Jolly, M.K., Tsarfaty, I., Onuchic, J., and Ben-Jacob, E. (2014). The three-way switch operation of Rac1/RhoA GTPase-based circuit controlling amoeboid-hybrid-mesenchymal transition. Sci. Rep. *4*, 6449.

Ibbetson, S.J., Pyne, N.T., Pollard, A.N., Olson, M.F., and Samuel, M.S. (2013). Mechanotransduction pathways promoting tumor progression are activated in invasive human squamous cell carcinoma. Am. J. Pathol. *183*, 930–937.

Johnsson, A.-K.E., Dai, Y., Nobis, M., Baker, M.J., McGhee, E.J., Walker, S., Schwarz, J.P., Kadir, S., Morton, J.P., Myant, K.B., et al. (2014). The Rac-FRET mouse reveals tight spatiotemporal control of Rac activity in primary cells and tissues. Cell Rep. *6*, 1153–1164.

Kardash, E., Reichman-Fried, M., Maître, J.-L., Boldajipour, B., Papusheva, E., Messerschmidt, E.-M., Heisenberg, C.-P., and Raz, E. (2010). A role for Rho GTPases and cell-cell adhesion in single-cell motility in vivo. Nat. Cell Biol. *12*, 47–53.

Komatsubara, A.T., Matsuda, M., and Aoki, K. (2015). Quantitative analysis of recombination between YFP and CFP genes of FRET biosensors introduced by lentiviral or retroviral gene transfer. Sci. Rep. *5*, 13283.

Kular, J., Scheer, K.G., Pyne, N.T., Allam, A.H., Pollard, A.N., Magenau, A., Wright, R.L., Kolesnikoff, N., Moretti, P.A., Wullkopf, L., et al. (2015). A negative regulatory mechanism involving 14-3-3ζ limits signaling downstream of ROCK to regulate tissue stiffness in epidermal homeostasis. Dev. Cell *35*, 759–774.

Li, A., Ma, Y., Yu, X., Mort, R.L., Lindsay, C.R., Stevenson, D., Strathdee, D., Insall, R.H., Chernoff, J., Snapper, S.B., et al. (2011). Rac1 drives melanoblast organization during mouse development by orchestrating pseudopod- driven motility and cell-cycle progression. Dev. Cell *21*, 722–734.

Lin, E.Y., Jones, J.G., Li, P., Zhu, L., Whitney, K.D., Muller, W.J., and Pollard, J.W. (2003). Progression to malignancy in the polyoma middle T oncoprotein mouse breast cancer model provides a reliable model for human diseases. Am. J. Pathol. *163*, 2113–2126.

Machacek, M., Hodgson, L., Welch, C., Elliott, H., Pertz, O., Nalbant, P., Abell, A., Johnson, G.L., Hahn, K.M., and Danuser, G. (2009). Coordination of Rho GTPase activities during cell protrusion. Nature *461*, 99–103.

Miyagi, C., Yamashita, S., Ohba, Y., Yoshizaki, H., Matsuda, M., and Hirano, T. (2004). STAT3 noncell-autonomously controls planar cell polarity during zebrafish convergence and extension. J. Cell Biol. *166*, 975–981.

Morton, J.P., Karim, S.A., Graham, K., Timpson, P., Jamieson, N., Athineos, D., Doyle, B., McKay, C., Heung, M.-Y., Oien, K.A., et al. (2010). Dasatinib inhibits the development of metastases in a mouse model of pancreatic ductal adenocarcinoma. Gastroenterology *139*, 292–303.

Myant, K.B., Cammareri, P., McGhee, E.J., Ridgway, R.A., Huels, D.J., Cordero, J.B., Schwitalla, S., Kalna, G., Ogg, E.L., Athineos, D., et al. (2013). ROS production and NF-κB activation triggered by RAC1 facilitate WNT-driven intestinal stem cell proliferation and colorectal cancer initiation. Cell Stem Cell *12*, 761–773.

Navas, C., Hernández-Porras, I., Schuhmacher, A.J., Sibilia, M., Guerra, C., and Barbacid, M. (2012). EGF receptor signaling is essential for k-ras oncogene-driven pancreatic ductal adenocarcinoma. Cancer Cell *22*, 318–330.

Neesse, A., Krug, S., Gress, T.M., Tuveson, D.A., and Michl, P. (2013). Emerging concepts in pancreatic cancer medicine: targeting the tumor stroma. Onco Targets Ther. *7*, 33–43.

Nimnual, A.S., Taylor, L.J., and Bar-Sagi, D. (2003). Redox-dependent down-regulation of Rho by Rac. Nat. Cell Biol. *5*, 236–241.

Nobes, C.D., and Hall, A. (1999). Rho GTPases control polarity, protrusion, and adhesion during cell movement. J. Cell Biol. *144*, 1235–1244.

Nobis, M., McGhee, E.J., Morton, J.P., Schwarz, J.P., Karim, S.A., Quinn, J., Edward, M., Campbell, A.D., McGarry, L.C., Evans, T.R.J., et al. (2013). Intravital FLIM-FRET imaging reveals dasatinib-induced spatial control of src in pancreatic cancer. Cancer Res. *73*, 4674–4686.

Noble, B.S. (2008). The osteocyte lineage. Arch. Biochem. Biophys. *473*, 106–111.

Pertz, O., Hodgson, L., Klemke, R.L., and Hahn, K.M. (2006). Spatiotemporal dynamics of RhoA activity in migrating cells. Nature *440*, 1069–1072.

Porter, A.P., Papaioannou, A., and Malliri, A. (2016). Deregulation of Rho GTPases in cancer. Small GTPases *7*, 123–138.

Prendergast, P.J., and Huiskes, R. (1996). Microdamage and osteocyte-lacuna strain in bone: a microstructural finite element analysis. J. Biomech. Eng. *118*, 240–246.

Rath, N., and Olson, M.F. (2012). Rho-associated kinases in tumorigenesis: re-considering ROCK inhibition for cancer therapy. EMBO Rep. *13*, 900–908.

Rath, N., Morton, J.P., Julian, L., Helbig, L., Kadir, S., McGhee, E.J., Anderson, K.I., Kalna, G., Mullin, M., Pinho, A.V., et al. (2017). ROCK signaling promotes collagen remodeling to facilitate invasive pancreatic ductal adenocarcinoma tumor cell growth. EMBO Mol. Med. *9*, 198–218.

Ritsma, L., Steller, E.J.A., Beerling, E., Loomans, C.J.M., Zomer, A., Gerlach, C., Vrisekoop, N., Seinstra, D., van Gurp, L., Schäfer, R., et al. (2012). Intravital microscopy through an abdominal imaging window reveals a pre-micrometastasis stage during liver metastasis. Sci. Transl. Med. *4*, 158ra145.

Ritsma, L., Steller, E.J.A., Ellenbroek, S.I.J., Kranenburg, O., Borel Rinkes, I.H.M., and van Rheenen, J. (2013). Surgical implantation of an abdominal imaging window for intravital microscopy. Nat. Protoc. *8*, 583–594.

Ritsma, L., Ellenbroek, S.I.J., Zomer, A., Snippert, H.J., de Sauvage, F.J., Simons, B.D., Clevers, H., and van Rheenen, J. (2014). Intestinal crypt homeostasis revealed at single-stem-cell level by in vivo live imaging. Nature *507*, 362–365.

Sahai, E., and Marshall, C.J. (2002). RHO-GTPases and cancer. Nat. Rev. Cancer *2*, 133–142.

Steele, C.W., Karim, S.A., Leach, J.D.G., Bailey, P., Upstill-Goddard, R., Rishi, L., Foth, M., Bryson, S., McDaid, K., Wilson, Z., et al. (2016). CXCR2 Inhibition Profoundly Suppresses Metastases and Augments Immunotherapy in Pancreatic Ductal Adenocarcinoma. Cancer Cell *29*, 832–845.

Thi, M.M., Suadicani, S.O., Schaffler, M.B., Weinbaum, S., and Spray, D.C. (2013). Mechanosensory responses of osteocytes to physiological forces occur along processes and not cell body and require αVβ3 integrin. Proc. Natl. Acad. Sci. USA *110*, 21012–21017.

Timpson, P., McGhee, E.J., Morton, J.P., von Kriegsheim, A., Schwarz, J.P., Karim, S.A., Doyle, B., Quinn, J.A., Carragher, N.O., Edward, M., et al. (2011). Spatial regulation of RhoA activity during pancreatic cancer cell invasion driven by mutant p53. Cancer Res. *71*, 747–757.

van Unen, J., Reinhard, N.R., Yin, T., Wu, Y.I., Postma, M., Gadella, T.W.J., and Goedhart, J. (2015). Plasma membrane restricted RhoGEF activity is sufficient for RhoA-mediated actin polymerization. Sci. Rep. *5*, 14693.

Vennin, C., Chin, V.T., Warren, S.C., Lucas, M.C., Herrmann, D., Magenau, A., Melenec, P., Walters, S.N., Del Monte-Nieto, G., Conway, J.R.W., et al. (2017). Transient tissue priming via ROCK inhibition uncouples pancreatic cancer progression, sensitivity to chemotherapy, and metastasis. Sci. Transl. Med. *9*, eaai8504.

Wang, X., He, L., Wu, Y.I., Hahn, K.M., and Montell, D.J. (2010). Light-mediated activation reveals a key role for Rac in collective guidance of cell movement in vivo. Nat. Cell Biol. *12*, 591–597.

Weissleder, R., Schwaiger, M.C., Gambhir, S.S., and Hricak, H. (2016). Imaging approaches to optimize molecular therapies. Sci. Transl. Med. *8*, 355ps16.

Wheeler, A.P., and Ridley, A.J. (2004). Why three Rho proteins? RhoA, RhoB, RhoC, and cell motility. Exp. Cell Res. *301*, 43–49.

Yang, H.W., Collins, S., and Meyer, T. (2016). Locally excitable Cdc42 signals steer cells during chemotaxis. Nat. Cell Biol. *18*, 191–201.

Yoshizaki, H., Ohba, Y., Kurokawa, K., Itoh, R.E., Nakamura, T., Mochizuki, N., Nagashima, K., and Matsuda, M. (2003). Activity of Rho-family GTPases during cell division as visualized with FRET-based probes. J. Cell Biol. *162*, 223–232.

Zhang, L., Luga, V., Armitage, S.K., Musiol, M., Won, A., Yip, C.M., Plotnikov, S.V., and Wrana, J.L. (2016). A lateral signalling pathway coordinates shape volatility during cell migration. Nat. Commun. *7*, 11714.